UNIVERSITY OF CALIFORNIA SAN DIEGO

Lymphatic Niches Regulate Asymmetric Stem Cell Dynamics in Tissue Regeneration

A Thesis submitted in partial satisfaction of the requirements
for the degree Master of Science

in

Biology

by

Vicky Yu-Wen Han

Committee in charge:

Professor Shiri Gur-Cohen, Chair
Professor Nan Hao, Co-Chair
Professor Alex Chaim
Professor Ye Zheng

2024

The Thesis of Vicky Yu-Wen Han is approved, and it is acceptable in quality and form for publication on microfilm and electronically.

University of California San Diego

2024

DEDICATION

This thesis is dedicated to my parents and family, whose unwavering support and faith in me have provided the foundation for this educational opportunity. Your endless encouragement and love have been the greatest motivation. I also dedicate this work to my esteemed advisor, Dr. Shiri Gur-Cohen, whose expertise, patience, and trust throughout my research were critical to my success. Finally, I dedicate this to my lab members, friends, and my significant other. Your selfless support and encouragement have helped me overcome numerous obstacles. This work would not have been possible without all of you.

TABLE OF CONTENTS

LIST OF FIGURES

ACKNOWLEDGEMENTS

I would like to express my gratitude to my chair advisor, Dr. Shiri Gur-Cohen for her endless and invaluable advice and encouragement during my undergraduate and master's studies. With countless discussions, guidance of troubleshooting processes, and continuous mental and educational support, her patience and immense knowledge have prepared me to be more confident in contributing to science research. Additionally, I would like to thank Dr. Robert Signer for providing the critical material, to allow me to investigate my research question in Chapter 4. I would also like to thank my committee members for being supportive throughout my thesis writing and defense. Last but not least, I would like to acknowledge all the members of the Gur-Cohen Lab, specifically, Madison Conte, Ananya Goyal, Katya Kazulina, and Sophia Vivar. Their daily selfless help, kind support, and suggestions have allowed me to successfully complete my project with confidence.

VITA

2023 Bachelor of Science in Molecular and Cell Biology, University of California San Diego

2024 Master of Science in Biology, University of California San Diego

ABSTRACT OF THE THESIS

Lymphatic Niches Regulate Asymmetric Stem Cell Dynamics in Tissue Regeneration

by

Vicky Yu-Wen Han

Master of Science in Biology

University of California San Diego, 2024

Professor Shiri Gur-Cohen, Chair
Professor Nan Hao, Co-Chair

Adult stem cells (SCs) are defined by their ability to self-renew to maintain a SC pool while preserving their potential to differentiate, ensuring tissue homeostasis. Yet, how SC fate decisions are dictated and synchronized across a tissue remains poorly understood. SCs are surrounded by and communicate with their supporting microenvironments, or "niches," for tissue regeneration. Recent evidence has revealed the lymphatic vascular system as a new niche entity for adult SCs

across epithelial tissues, including hair follicle stem cells (HFSCs) in the skin. However, whether lymphatic vasculature can instruct SC fate decisions in tissue renewal is unknown. Here, we investigate how HFSC fate decisions and differentiation potential are guided by their spatial proximity to lymphatic niches during homeostatic tissue regeneration. Using deep 3-dimensional imaging of the regenerated hair follicles (HFs), coupled with genetic lineage tracing and conditional lymphatic ablation models, we identify an asymmetric lymphatic architecture surrounding the HFSCs across the horizontal axis of the follicle. Through tracking SC proliferation rates and detailed temporal lineage tracing, our findings reveal a clonal imbalance in the regenerated HF. We demonstrate the most regenerating SCs exhibit earlier cell divisions and originate near lymphatic capillaries. In contrast, SCs from later division waves, which reside farther from the lymphatics, primarily maintain self-renewal rather than contribute to differentiation and tissue regeneration. This study provides a further direction to understand the lymphatic-stem cell duet in tissue regeneration, which could have important clinical implications for stem cell transplantation and therapeutic intervention to advance wound response in degenerative pathologies.

INTRODUCTION

Adult stem cell (SC) self-renewal and regenerative capacity empower organisms to extend their lifespan despite tissue injury, ensuring the preservation of essential functions and operations within their native organs to uphold tissue homeostasis (Mimeault & Batra, 2008; Tian et al., 2023). These adult stem cells encode tissue-specific identity and cell proliferation in their particular environment (Marusyk & DeGregori, 2008). However, the regenerative potential of stem cells deteriorates with age (Goodell & Rando, 2015), while excessive stem cell activation can fuel tumor initiation and cancer progression by leveraging their inherent stemness properties (Aponte & Caicedo, 2017; Batlle & Clevers, 2017; Laplane & Solary, 2019). Unrevealing the mechanisms that regulate stem cell activity throughout life is crucial to understanding why tissues gradually lose their capability for wound repairs and become increasingly susceptible to tumor formation with age.

In the skin, the hair follicle (HF) exhibits defined regions where SCs are localized in an epithelial compartment, the bulge, along with the immediate differentiated progenitors, called hair germ (HG), vertically residing below (**Fig. 1A**; Cotsarelis et al., 1990; Morris et al., 2004; Rompolas et al., 2013). A hair follicle stem cell (HFSC) located in the upper bulge is programmed to a specific fate including quiescent retention, self-renewal, or identity loss (Rompolas et al., 2013). Previous work has demonstrated that cells closer to the HG have a higher potential to generate precursors or differentiate (Hsu et al., 2011; Jahoda et al., 1984; Rompolas et al., 2012, 2013). While the behavior of individual SCs in different positions in the SC niche has not been fully determined, the varying cell populations in the HFs work in synchrony to fuel hair regeneration.

HF regeneration is typically performed with a distinct cycle, allowing the precise timing of the resting phase (telogen; Tel), activation phase (anagen: Ana), and regression phase (catagen; Cat) to be anticipated (Alonso & Fuchs, 2006; Rompolas et al., 2013). It was previously shown that during the anagen phase, HFSCs in the bulge region empower hair growth to generate a new bulge in a cycle, activated by the mesenchymal cells, called dermal papilla (DP), which are in contact with the HG (**Fig. 1A**; Hsu et al., 2011). Specifically, HFSCs are activated during Ana II-III (Gur-Cohen et al., 2019), and resume quiescent after a complete hair cycle ends. The distinguished and regular characteristics of HFSCs provide a powerful model to study SC regeneration potential within their native environments.

While most adult SCs are confined to regenerating their specific lineage, some possess the unique ability to broaden their tissue-specific fate and functions in response to injury; for instance, HFSCs can shift their fate and differentiate into epidermal stem cells to facilitate wound repair in skin tissue (Blanpain & Fuchs, 2014; Ito et al., 2005). Interestingly, growing evidence suggests the intriguing possibility that stem cell fates can change depending on their close interactions with their dynamic surrounding microenvironment, or "niche" (Ferraro et al., 2010; Fuchs & Blau, 2020; Morrison & Spradling, 2008; Prager et al., 2019). Yet, the precise mechanisms by which niche dynamism instructs stem cell bi-potent characteristics, allowing tissue-resident adult stem cells to generate both HF and epidermal lineage, remain poorly understood. Equally unclear is whether non-skin epithelial lineages, such as those in the lung and intestine, possess the capacity to alter their fates and expand their regenerative strategies when exposed to specialized skin niches.

The adult vascular system has been recognized to play a key role in maintaining and expanding SC across various biological systems (Putnam, 2014). Previous studies have demonstrated the association of blood endothelial cells with bone marrow homeopathic stem cells

(HSC), thereby creating a niche environment that supports the maintenance of HSCs through the secretion of angiocrine factors (Kiel et al., 2005; Kusumbe et al., 2016). While the blood vasculature network has been widely studied, another vascular system, the lymphatic vascular system, has emerged as a new niche for stem cells (Gur-Cohen et al., 2019; Peña-Jimenez et al., 2019). Historically, lymphatic vascular systems have been recognized for fluid transport and immunosurveillance for a long period (Oliver, 2004; Tammela & Alitalo, 2010); nevertheless, in the skin, the lymphatic vasculature network serves as a new and dynamic niche for HFSCs (Gur-Cohen et al., 2019; Peña-Jimenez et al., 2019). Furthermore, lymphatics were found to form a hub for SC factors to regulate regenerative potential in the intestine epitheliums, representing that lymphatic loss of function induced precocious regeneration (Goto et al., 2022; Niec et al., 2022; Palikuqi et al., 2022).

Interestingly, SCs, such as HFSCs, not only receive signals from their niche but also provide a cue to their niche to build up a supportive microenvironment for homeotic regeneration (Gur-Cohen et al., 2019; Li & Tumbar, 2021). HFSCs express angiopoietin-like protein 7 (Angptl7), stimulating lymphatic drainage, and Angptl4, inducing lymphatic-HFSCs disassociation for drainage reduction during the resting phase and the activated phase, respectively (Gur-Cohen et al., 2019). This demonstrates the ability of SCs to reshape their own niches. Nevertheless, whether the spatial interactions of lymphatic SC niche and HFSCs can instruct stem cell fate decisions is yet to be determined.

Here, we set to explore how direct communication between HFSCs and the surrounding lymphatic vessels influences tissue regeneration. Our goal is to define how the spatial position of the lymphatic niche carries out HFSC fate decisions during tissue renewal and determine whether lymphatics may direct stem cells' bi-potent cell behavior in the act of tissue repair. Using the

CreER/loxp inducible reporter system for tracing stem cell lineage fate and history, coupled with EdU tracing for cell proliferation rate and deep tissue imaging, our preliminary studies discover that the lymphatic vessel is asymmetrically positioned along each HF. HFSCs that are in close contact with lymphatics are more likely to exhibit distinct hair regeneration and differentiation, whereas those distant from lymphatics tend to remain within the bulge, contributing less to tissue regeneration. Using a conditional iDTR mouse model for lymphatic ablation, we further confirm that lymphatic restrict stem cell activation and that their disassociation triggers stem cell activation (Gur-Cohen et al., 2019). Our findings define tissue regeneration as an asymmetric event, where stem cells unequally contribute to the regenerated organ depending on their association with the lymphatic niche, and illuminate how downstream SC niche cues can provide inductive feedback to expend SC potency for tissue repair.

Chapter 1 ASYMMETRIC STEM CELL ACTIVATION IN THE REGENERATED HAIR FOLLICLE

To dissect the properties of bulge SC descendants along the regenerated HF, we first performed a detailed temporal cell cycle pulsing and long-term SC chasing by employing label-retaining assays to trace HFSC proliferation rates and histories using 5-ethynyl-2'-deoxyuridine (EdU) incorporation from the first resting state (telogen: 'Tel') to the HFSC activation state (anagen: 'Ana') in the mouse back skin (**Fig. 1A -B**). EdU is a thymidine analog that can integrate into DNA during cell proliferation (Buck et al., 2008). During the 'pulse' phase, cells that undergo replication will incorporate EdU and be labeled (**Fig. 1B, EdU-Pulse**). In contrast, during the 'chase' phase, rapidly proliferating cells gradually dilute their EdU labels with each division, while slow-cycling cells retain the labels (**Fig. 1B, EdU-Chase**; Buck et al., 2008; Chen et al., 2014; Cotsarelis et al., 1990; Zhang et al., 2015).

From telogen to early anagen (Ana I-II), the lack of EdU-labeled cells in the bulge regions confirmed that HFSCs remained in a quiescent state (**Fig. 1C, left**). Upon reaching anagen-III, as HFSCs became activated, we observed an asymmetric proliferation pattern, with the anterior bulge showing greater EdU incorporation compared to the posterior side (**Fig. 1C, mid**). The unequal SC activation was consistently observed in the late Ana-III (**Fig. 1C, right**), revealing a unilateral wave of HFSC activation during the initiation of hair regeneration.

We next sought to investigate whether the observed differences in HFSC proliferation were associated with the proximity of SC to their surrounding lymphatic niches. Notably, the anterior region, which showed a faster onset of EdU incorporation, was closely associated with $LYVE1^+$ lymphatic vessels (**Fig. 1D**). In contrast, the posterior side of the follicle, which is spatially distant from the lymphatic vessels, exhibited fewer EdU^+ cells, indicating a slower HFSC proliferation

activity (**Fig. 1D**). These results suggested the clues of lymphatic niches may play a role in guiding HFSCs towards asymmetric regenerative potential.

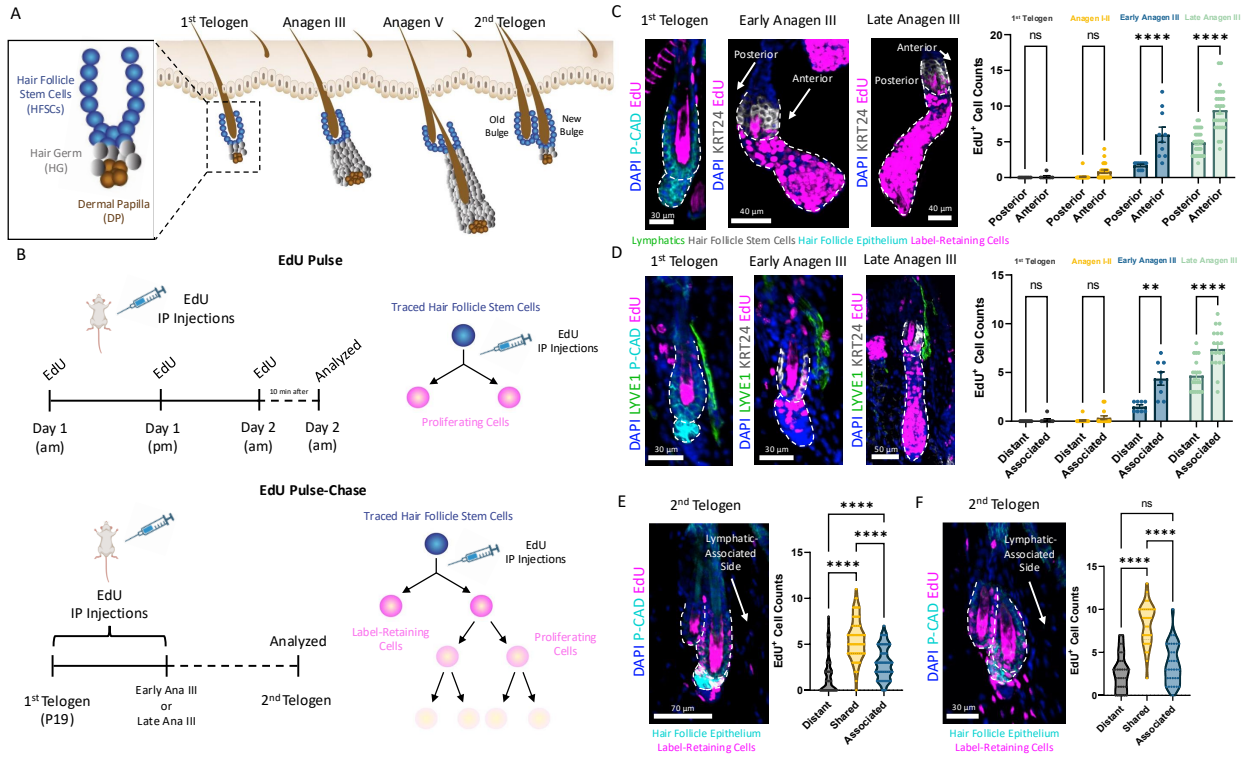

Figure 1: Hair follicle stem cells have asymmetric proliferation rates instructed by their lymphatic niche.

(**A**) Stages in the hair cycle, and essential components of the hair follicle (HF) including hair follicle stem cells (HFSCs, located in the bulge region), hair germ (HG), and dermal papilla stromal cells (DP). (**B**) Timeline of the experimental model was performed accordingly: **EdU Pulse**: EdU was injected 24h, 12h, and 10 min before analyzing the mice (a total of 3 injections to target cycling stem cells). **EdU Pulse-Chase**: EdU was injected twice a day from 1st telogen until either early anagen III or late anagen III, and the mice were chased and analyzed at the end of the 2nd hair cycle when stem cells returned to quiescence. (**C**) Dispase-treated whole mount immunofluorescence demonstrating EdU^+ proliferating cells (magenta), KRT24 (HFSCs, white), and DAPI along different stages in the hair cycle. *2-way ANOVA (+SEM); 1st telogen: ns, $n = 3$; anagen I-II: ns, $n = 4$; early anagen III: $p < 0.0001$, $n = 2$; late anagen: $p < 0.0001$, $n = 2$. (**D**) 2D cryostat-section immunostaining of EdU^+ proliferating (magenta) and $KRT24^+$ (white) cells and their spatial proximity to $LYVE1^+$ lymphatic (green) along the horizontal axis of the HF. *2-way ANOVA (+SEM); 1st telogen: ns, $n = 2$; anagen I-II: ns, $n = 3$; early anagen III: $p = 0.001$, $n = 2$; late anagen: $p < 0.0001$, $n = 2$. (**E-F**) 2D cryostat-section immunostaining and quantification of EdU^+ label-retaining (magenta) and $KRT24^+$ (white) HFSCs when pulsed-chased at either (**E**) early anagen III, *$p < 0.0001$, one-way ANOVA (+SEM), $n = 6$; or (**F**) late anagen III, *$p < 0.0001$, one-way ANOVA (+SEM), $n = 4$. Note the shared epithelium as SC that originated from SC associated with lymphatics in the 1st hair cycle.

To further investigate the spatial regulation of the lymphatic vascular network and its impact on the unequal proliferation dynamics of HFSCs, we EdU-labeled HFSCs from the first telogen phase, tracking them through either early Ana-III or late Ana-III. We then pulse-chased these proliferating cells into the second resting phase, where a new bulge forms and the HG retracts to the newly formed bulge within the complete hair cycle (**Fig. 1A-B**). Pulse-chase experiments during early Ana-III, when lymphatic-associated SCs were first activated, and late Ana-III, when lymphatic-distant cells also began to proliferate (**Fig. 1D**), revealed that slow-cycling cells predominantly resided in the middle epithelial layer (the shared epithelial layer), originating from lymphatic-associated regions during the pulse of the early cycle (**Fig. 1E-F**). The asymmetric spatial association of lymphatics and differential HFSC proliferation rates suggested the intriguing possibility that stem cell-lymphatic communication may instruct distinct cell fate decisions during hair regeneration. Our results suggested that lymphatic-associated SCs were activated more swiftly than their distant counterparts (**Fig. 1C-D**), yet maintained EdU labeling. This indicates a slow cycling rate, and the direct contribution to forming the new SC bulge through self-renewal, thereby sustaining the SC pool (**Fig, 1E-F**). As SC activation began asymmetrically, lymphatic-distant HFSCs exhibited the lowest EdU incorporation during the chase period (**Fig. 1E**). It is plausible that EdU-negative cells observed during the pulse phase represented cells that could never enter the cell cycle, or were lost from the SC niche, evidenced by the EdU-pulse assay showing lymphatic-distant HFSCs performing a delayed initiation of proliferation in early Ana-III (**Fig. 1C-D**). We, therefore, set out to explore the significance of lymphatic niche positioning to SC fate by utilizing an *in vivo* lineage approach.

Chapter 2 STEM CELLS CONTRIBUTE UNEQUALLY TO THE REGENERATED FOLLICLE

To genetically mark and trace HFSCs and progenitors in the bulge, we use mice harboring *Sox9-CreER*, in addition to *Rosa-stop-Brainbow* reporter alleles (or *Rosa-stop-EYFP* reporter alleles). In these mice, the $Sox9^{+}$ HF clones will express muti-fluorescent proteins after the administration of tamoxifen (TAM). Upon Cre recombinase activation, each copy of a *Brainbow* construct recombines in a stochastic manner to express either *nGFP, EYFP*, *dTomato*, or *Cerulean*. We traced individual HF clones labeled with a HFSC-specific marker keratin 24 (KRT24) from Tel to Ana-III-V when HFSCs were activated and initiated HF elongation and regeneration (**Fig. 2A-B**). In Tel, both bulge sides represented a single to triple clone labeling in the bulge region, suggesting that the labeling efficiency was similar between lymphatic-associated and lymphatic-distant stem cells (data not shown). In Ana-III, our genetic lineage tracing showed that more than 80% of the regenerated HFSC clones originated from the lymphatic-associated side, whereas HFSC clones from the lymphatic-distant side made a smaller contribution to the regenerated follicle (**Fig. 2C-D**). Notably, retaining HFSC clones were distributed evenly across the bulge, suggesting non-regenerating HFSCs were uniformly distributed across the horizontal axis of the follicle (**Fig. 2C**). These results further highlight the unique capabilities of lymphatic-associated stem cells in driving both self-renewal and regeneration, as previously indicated by the label-retaining assays (**Fig. 1E-F**).

Previous publications have demonstrated that in the regenerated HF, the slow-cycling cells will survive through the catagen phase and give rise to both the differentiated progenitor HG and a newly formed bulge, turning into the fuel of SCs for next-cycle performance (Hsu et al., 2011). In alignment with our pulse-chase findings, HFSC clones situated near lymphatic niches expanded

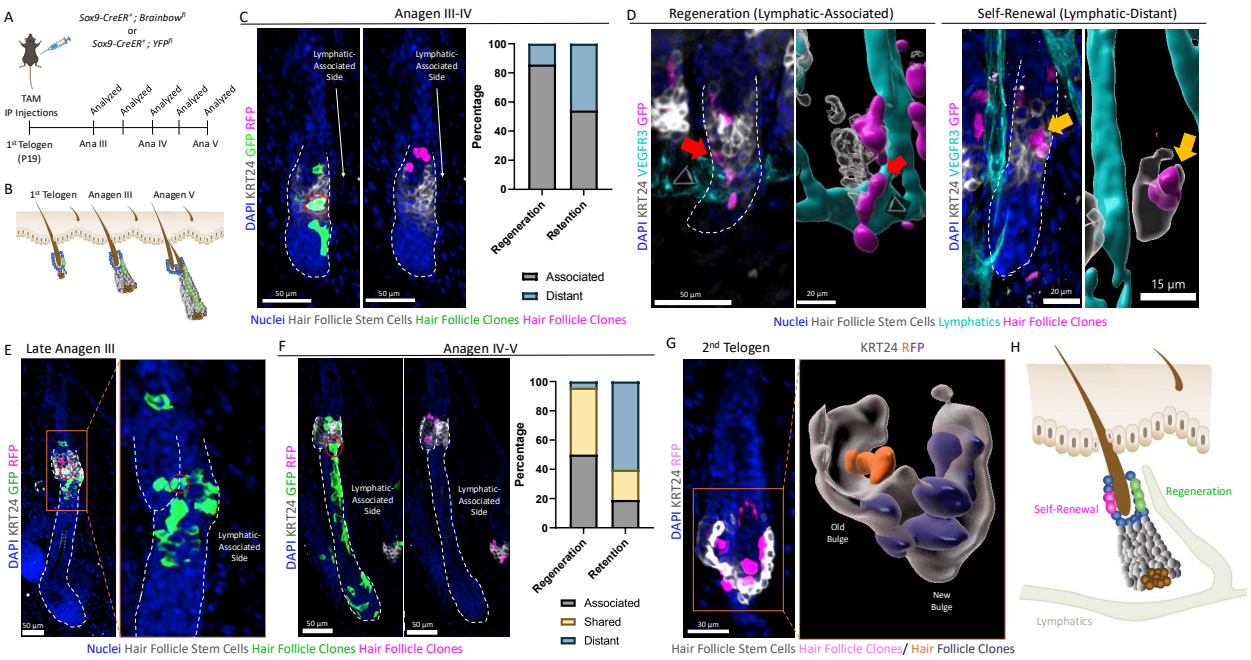

Figure 2: Hair follicle stem cells have asymmetric fate decisions instructed by their lymphatic niche.

(**A**) Timeline of the experimental model and Tamoxifen (TAM) induced Sox9^{+} HF multi-color clones during stem cell activation. (**B**) Scheme of Sox9^{+} HF multi-color clone fates from 1st telogen to anagen. (**C**) Lineage clone tracing of *Sox9-CreER^{+};Brainbow^{fl}* transgenic mouse model at anagen III-IV, $n = 6$ (HF $n = 28$). (**D**) Representative image of *Sox9-CreER^{+};YFP^{fl}* clones using 3D deep imaging of HFs at anagen III, demonstrating lymphatic-associated KRT24^{+} GFP^{+} clone that contributed to the regenerated HF (red arrows) or lymphatic-distant KRT24^{+} GFP^{+} clone that retained in the bulge and did not contribute to regeneration (yellow arrows). (**E-F**) representative image of a HF clone (circled in red) migrated from the shared KRT24^{+} epithelium to the lymphatic-associated side, followed by downward migration for regeneration. Lymphatic-distant RFP^{+} clones retained and did not contribute to the down growth of the HF, $n = 2$ (HF $n = 27$). (**G**) Representative 3D deep imaging of *Sox9-CreER^{+};Brainbow^{fl}* HF clones traced from the 1st telogen to the 2nd telogen of the HF. Each color (orange and purple) represents an individual clone: the retained clone, marked in orange, is localized to the old bulge (lymphatic-distant), while the migrated clone (lymphatic-associated) is highlighted in purple. (**H**) HFSC embraces asymmetry to regenerate the follicle. Summary schema.

to create a new bulge, marked by the expression of the HFSC marker KRT24. These clones also demonstrated a downward pattern, contributing to the regeneration of the follicle (**Fig. 2E**). Next, we carefully quantified the HFSC clone fate decisions relative to their proximity to the lymphatic

niches as hair regeneration progresses. Remarkably, HFSC clones on both the shared epithelial layer between the old and new bulges and the lymphatic-associated sides contributed to more than 90% of regenerated HF, while lymphatic-distant clones retained within the bulge without contributing to regeneration, but maintaining their stem cell identity (**Fig. 2F**). We continued tracing the HFSC clones to the next telogen phase and observed that the HFSC clone (labeled in purple) on the shared epithelial area established a migration pathway to the new bulge at the second resting stage, consistent with our pulse-chase observations (**Fig. 1E-F; Fig. 2G**). These findings highlighted that HFSCs in close proximity to lymphatics were uniquely positioned to initiate new bulge formation after a complete regeneration cycle. In contrast, stem cells that were distant from the lymphatic niche exhibited minimal activity, contributing primarily to self-renewal with limited proliferative capacity (**Fig. 2H**).

Chapter 3 LYMPHATIC DISRUPTION RESULTS IN HYPERPLASIA OF HAIR REGENERATION BUT MAINTAINS HAIR FOLLICLE STEM CELL ASYMMETRIC BEHAVIOR

The unique fate and developmental potential of lymphatic-associated SCs may be shaped by molecular asymmetries in gene expression and epigenetic modifications. It may be possible that SCs are molecularly heterogeneous, initiating distinct terminal differentiation programs based on a spatially pre-determined transcriptional landscape. To distinguish whether SCs are molecularly heterogeneous, we analyzed referenced SCs from the bulge at the second resting phase at the single-cell level. Consistent with the traditional view, SC markers like KRT24 and transcriptional factors such as Sox9 were molecularly homogeneous within the bulge stem cell population (**Fig. 3A; Sox9 data not shown**; Gur-Cohen et al., 2019; Yang et al., 2017). This finding raises the intriguing possibility that SCs may adopt spatially defined fates based on pre-existing potential, rather than being driven by a molecular heterogenous predetermination.

To comprehend how lymphatic niches regulate HFSCs during regeneration, we conducted a *Prox1-CreER*$^{+}$*;iDTR*^{fl} knock-in mouse model to locally perturb lymphatic vessels in the skin from telogen to early anagen. The administration of TAM enabled the expression of Cre recombinase Prox1 lymphatic endothelium, along with the Cre-inducible diphtheria toxin (DT) receptor, leading to lymphatic ablation upon DT introduction (Gur-Cohen et al., 2019). To assess HFSC proliferation dynamics in precocious Ana caused by lymphatic perturbation (Gur-Cohen et al., 2019), we next adapted the EdU label-retaining assay and traced them to P50 (**Fig. 1B; Fig. 3B**). When HF regeneration proceeded with normal lymphatic niche support, the HFs entered the regression phase when hair differentiation ceases (catagen; **Fig. 3C**; Alonso & Fuchs, 2006). The EdU^{+} HFSCs retained the most on the shared epithelial area between the old bulge and the emerging new bulge (**Fig. 3C-D**), consistent with our previous EdU pulse-chase assay (**Fig. 1E-**

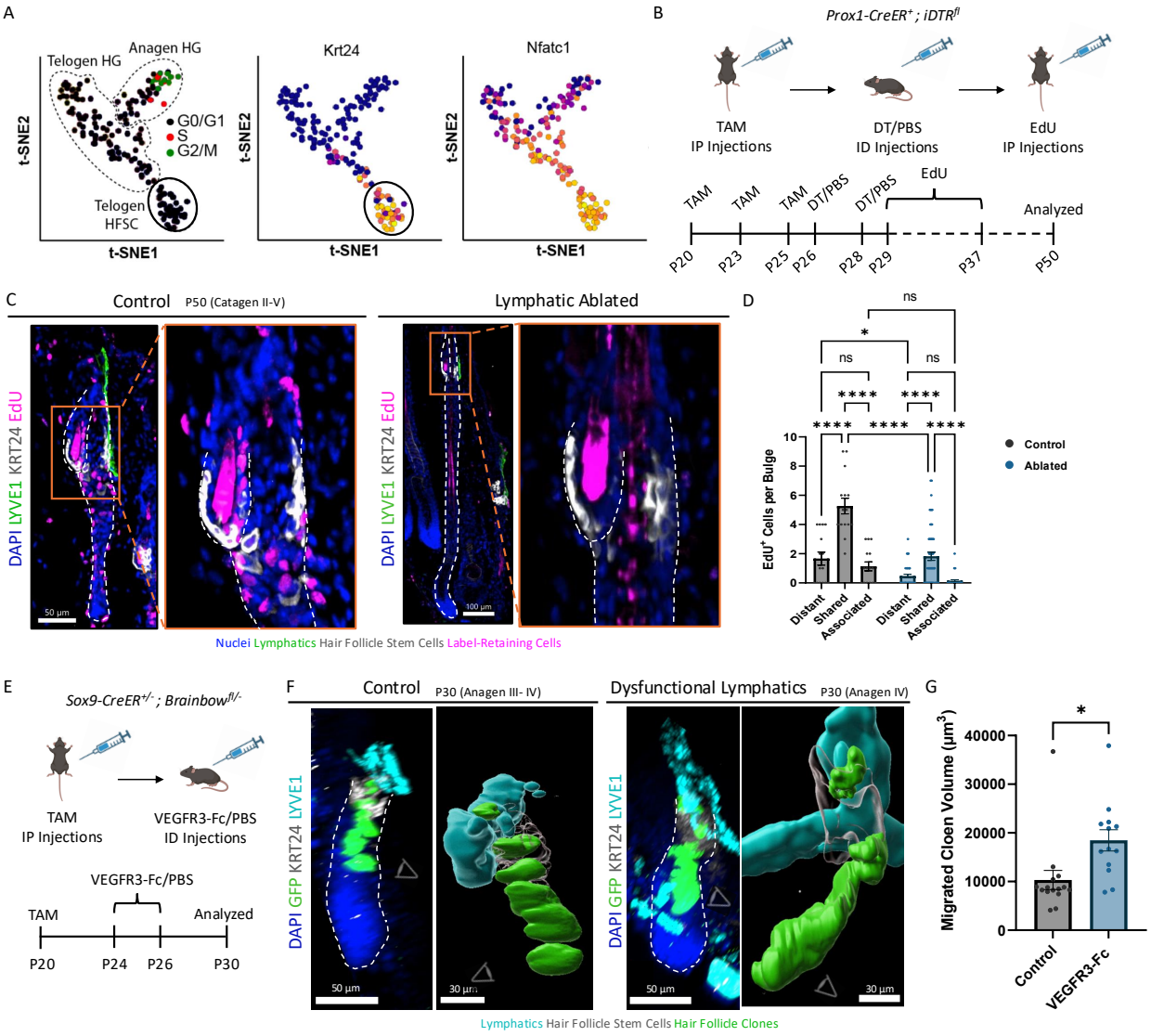

Figure 3: Loss of asymmetric fates in hair follicle stem cells when stem cell-lymphatic niche communication is perturbed.

(**A**) Single-cell RNA sequencing unbiased clustering at telogen of sorted HF cells. HFSCs in telogen (solid circled) are indicated by the SC markers Krt24 (GEO: GSE90848; Gur-Cohen et al., 2019). (**B-D**) EdU Pulse-Chase assay following lymphatic vessel ablation, induced by diphtheria toxin (DT) in *Prox1-CreER*$^{+}$*;iDTR*^{fl} mice, with TAM injections administered during the early stage of the hair activation cycle and chased at P50. *p < 0.05, two-way ANOVA (+SEM), control: $n = 2$, experimental: $n = 4$. (**E-G**) Lineage tracing of Sox9^{+} HF multi-color clones in *Sox9-CreER*$^{+/-}$*;Brainbow*$^{fl/-}$ mice followed by VEGFR3-Fc injections during the early stage of hair activation cycle. *p < 0.05, unpair t-test (+SEM), control: $n = 1$, experimental: $n = 1$.

F). Notably, although lymphatic ablation during the HFSC activation phase led to a significant decrease in EdU^+-retaining stem cells on all sides, indicating rapid proliferation, the asymmetric proliferation choices were still maintained, with the greatest label-retaining cells located in the shared area (**Fig. 3C-D**). The results suggested there were signals originating from lymphatics that had already been reimposed to the asymmetric behavior.

Employing another experimental model for lymphatic disruption, we injected the VEGFR3-Fc decoy receptor into TAM-induced *Sox9-CreER*$^+$*;Brainbow*^{fl} transgenic mice (**Fig. 3E**). The soluble VEGFR3-Fc receptor inhibits VEGFR3 signaling, which is crucial for the proliferation and survival of lymphatic endothelial cells (Gur-Cohen et al., 2019; Mäkinen et al., 2001), leading to dysfunctional lymphatic vessels. Compared to the control group, the HFSC clones that contributed to hair regeneration were enlarged in volume in the lymphatic dysfunctional group (**Fig. 3F**), indicating abnormal hyperplasia, consistent with the previous evidence and lymphatic ablation model (Gur-Cohen et al., 2019). These results provided further evidence of the essential regulation of the HFSC-lymphatic niche communication during tissue regeneration.

Chapter 4 LYMPHATIC-ASSOCIATED STEM CELLS SYNTHESIZE MORE PROTEIN DURING HAIR REGENERATION

Our data indicated that while SCs are molecularly homogeneous at the mRNA level, functional assays revealed that their fate determination varied distinctly along the horizontal axis of the HF (**Fig. 1-2**). To investigate whether lymphatic-associated SCs influence these distinct fate decisions by regulating global protein synthesis during the onset of tissue regeneration, we measured global protein synthesis rates by quantifying the incorporation of OP-puromycin (OP-puro) into nascent proteins (**Fig. 4A**; Liu et al., 2012). During the HF resting state, SCs uniformly displayed comparable Op-Puro intensity, indicating a similar protein synthesis rate (**Fig. 4B, left**). However, an asymmetry in protein synthesis emerged between the two sides of the bulge region during early Ana, with higher Op-Puro intensity observed in the lymphatic-associated HFSCs (**Fig. 4B, right**). These findings suggested molecular-level crosstalk between HFSCs and the lymphatic niche during stem cell activation.

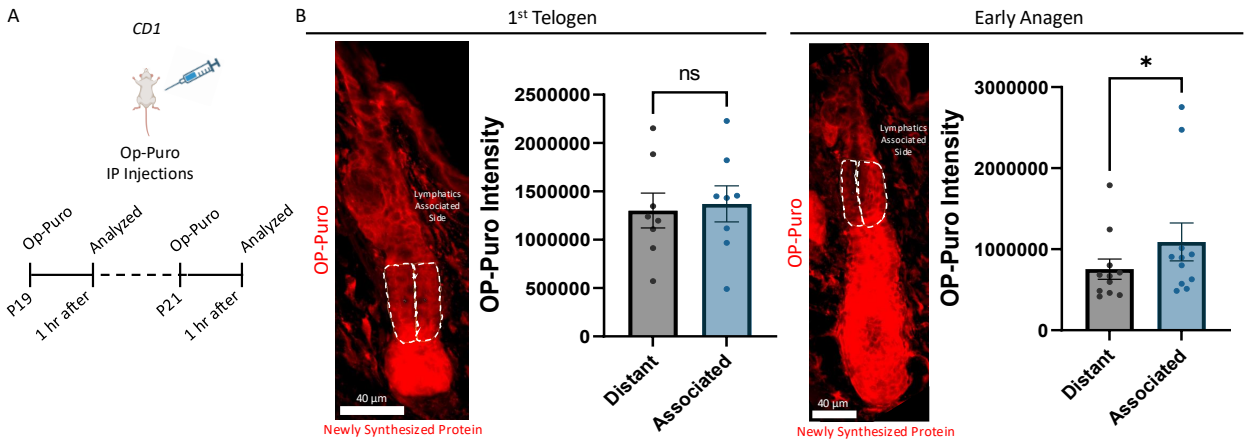

Figure 4: Hair follicle stem cell-lymphatic niche communication is associated with unequal protein synthesis during stem cell activation.

(**A**) Timeline of the experimental model for Op-Puro translational rate assay at 1st telogen and early anagen. (**B**) Representative images and quantification of Op-puro incorporation into the regenerated HF cells, demonstrates unequal protein synthesis rate along the bulge horizontal axis. *p < 0.05, paired T test (+SEM), $n = 1$ (1st telogen) and $n = 1$ (early anagen).

Chapter 5 LYMPHATIC NICHES DRIVE STEM CELL BI-POTENT BEHAVIOR TO REGENERATE TISSUE LOST

Understanding the essential regulations between the lymphatic vascular network and HFSCs during tissue regeneration and fate determination, we sought to explore whether the lymphatic vasculature also served as stem cell niches for stem cell fate flexibility during tissue regeneration. To investigate the effect of lymphatic niches on the esophageal epithelium plastic behavior, we obtained esophageal epithelium from a *UBC-GFP* mouse which expressed green fluorescent protein directed by the human ubiquitin C promoter, and the skin dermis (HFs and skin epidermis removed) derived from *Prox1-CreER*$^{+}$*;iDTR*^{fl} control or lymphatic ablated skin. We then created an esophageal epithelium-skin dermis co-culture tissue (**Fig. 5A**; Bejar et al., 2021). In the control group, where the lymphatic vasculature system remained intact, we observed robust GFP^{+} HF formation that was positive to the KRT24 HFSC marker (**Fig. 5B, left**). This finding suggested that the GFP^{+} esophageal epithelium exhibited notable fate flexibility, successfully adopting the HF identities. However, when GFP^{+} esophageal epithelium was cultured on the skin dermis with a compromised lymphatic network, the formation of complete GFP^{+} regenerated HFs was markedly absent, indicating a failure in plasticity, likely due to the absence of supportive niches during tissue regeneration (**Fig. 5B, right**). These results revealed the novel role of lymphatic niches in directing SC fate decisions much beyond the epidermis, enabling the transformation of esophageal identity into HF lineage to repair and replace the loss of epidermal tissue.

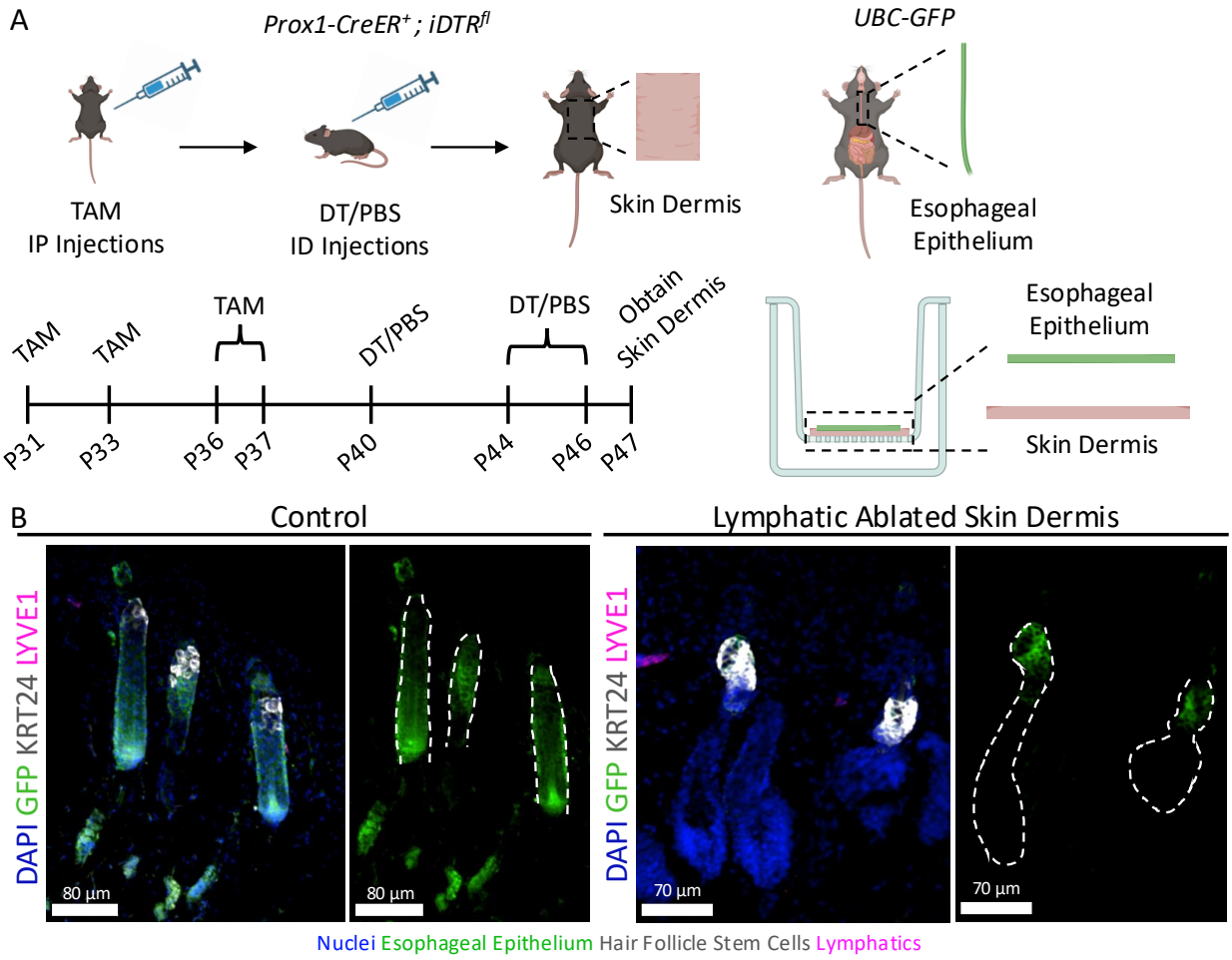

Figure 5: The lymphatic niche promotes esophageal epithelium plastic cell behavior in a novel esophagus-dermis co-culture system.

(**A**) Experimental model: skin dermis was obtained from *Prox1-CreER*$^{+}$*;iDTR*^{fl} control or lymphatic-ablated skin, and esophageal epithelium was sourced from ubiquitous *GFP* mice. The dermis was separated from the epidermis, and the basal esophagus was separated from the underlying muscles using dispase + EDTA. The isolated GFP^{+} esophageal epithelium was then placed on top of the control or lymphatic-ablated dermis, and co-culture organotypic models were analyzed 10 days after the initial culturing. (**B**) GFP^{+} esophageal epithelial cells changed their fate and assumed HF identity when cultured on top of the control dermis, but not on the lymphatic-ablated dermis.

DISCUSSION

In this study, our data strongly suggests that the spatial proximity between stem cells and the lymphatic niche is crucial in directing stem cell fate. We uncovered a novel asymmetric lymphatic architecture positioned around the stem cell bulge on the horizontal axis, which dictates the unequal fate choices and differentiation potential during tissue regeneration. These findings extend beyond homeostatic HF regeneration and may provide fundamental knowledge of how asymmetric regulation benefits SC fate decisions and SC flexibility in response to tissue injury, cancer progression, and other severe diseases.

Previous studies have shown that the germ line stem cells (GSCs) in *Drosophila*, exhibit unequal differentiation fates, in which merely GSCs in close contact with their niche, called hub cells, have the capacity for maintaining stem cell identity, whereas SC-niche dissociation induces differentiation capability (Fuller & Spradling, 2007; Yamashita et al., 2010). Furthermore, in the 2-cell stage embryo, it has been evident that only one of the 2-cell blastomeres contributes to the later progeny, the epiblast cells, while the other blastomere eventually becomes the yolk sac, indicating an asymmetric differentiation during the developmental stage as well (Junyent et al., 2024). Our findings provide significant insights into the asymmetric interactions between SCs and their niche, specifically highlighting the role of lymphatics in driving unequal fate decisions and regeneration potential. While the precise cues and mechanisms guiding these asymmetric choices remain to be fully elucidated, our discovery of lymphatic as a pivotal component of this niche opens new avenues for exploring SC behavior. This understanding not only advances the field of stem cell biology but also has potential implications for regenerative medicine, where harnessing or modulating these asymmetric signals could improve tissue repair and regeneration strategies.

Lymphatic development and functions are regulated both by biomedical signals, such as VEGFs and Ccbe1 for structural formation, and biomechanical factors, like FAT4, which is essential for fluid-flow response in lymphatic elongation (Oliver et al., 2020). While the SC fates and tissue regeneration are dictated by the functional lymphatic niche proximity, as suggested by our study, it is crucial to understand the dynamics of the lymphatic vascular system function and integrity, and angiogenic and lymphogenic factors impact normal lymphatic functions with regard to SC asymmetric regenerative potential. External regulation within a native SC-niche environment may provide opportunities not only for hair growth induction in hair loss patients but also for reprogramming native SC identity to repair tissue wounds, improve aged conditions, or inhibit tumor progression. This research extends the foundational understanding of stem cell-niche interaction, providing further directions for maintaining and harnessing healthy stem cell capabilities.

Some limitations of this research include the lack of a stem cell-specific tracing model. In this research, we conducted genetic lineage tracing using the *Sox9-CreER* system, in which the expressed clones represented all hair follicle cell lineages including the SCs and the differentiated progenitors. While we only analyzed the $Sox9^{+}$ clone that emerged from the bulge within the $KRT24^{+}$ region, this limitation could lead to the possibility of capturing non-SC $Sox9^{+}$ clone pathways originating from other HF progenitors such as HG. For our future proposed studies, we will elaborate a HFSC-specific genetic model, such as the *Krt19-CreER* system for further confirmation of stem cell regeneration potential. Additionally, the lack of long-term protein incorporation and proteomic sequencing analysis limited further insights into whether an asymmetric regulation at the molecular level is presented throughout a complete hair cycle. Further studies include a long-term protein synthesis screening *in vivo*, and a detailed mechanism

investigation of how the lymphatic dynamics instruct HFSC fate switches at cellular and molecular levels during hair regeneration.

Taken together, my research positions lymphatic vessels as an asymmetric niche entity for the regenerating HFSCs, and suggests that lymphatic cues may provide inductive signals for SC fate flexibility and identity throughout normal hair regeneration and tissue repair. Exploring how SCs respond to their ever-changing vascular niches could provide insights into questions like why it is advantageous for tissue renewal to adopt an asymmetric regenerative program that shields against oncogenic stressors accumulating in the SC niche after injury. Understanding these mechanisms could enable us to leverage this asymmetry to engineer more resilient tissues for transplantation.

MATERIALS AND METHODS

Mice strains and housing

CD1 wild-type, and *Sox9-CreER^{+};Brainbow^{fl}*, *Sox9-CreER^{+};YFP^{fl}*, *Prox1-CreER^{+};iDTR$^{fl/fl}$*, and *UBC-GFP* (C57BL/6 background) were purchased from The Jackson Laboratories. Mice used for experiments were maintained by the Animal Care Program of the University of California, San Diego (UCSD), and procedures were performed with the Institutional Animal Care and Use Committee (IACUC)-approved protocols. All mice were housed in an environment with controlled temperature and humidity, on 12-hour light:dark cycles, and fed with regular rodent chow. The numbers of animals used for experiments presented in each figure are indicated in the legends as n = x mice per group, per time point analyzed.

Hair cycle timing

Hair cycles vary regarding mouse strains, sexes, and litter sizes. The stages of hair cycles were determined based on the HFSC activation time points and HF morphology instead of exact mouse ages. For the timepoint-check purpose, a back skin biopsy of an individual mouse or mice within the same litter was acquired and incubated (dermis side down) on 2.5 U/ml dispase II (Fisher Scientific) + 19.23 mM EDTA (Fisher Scientific) for at least 2 hours at 37°C on a shaker. HFs were separated from the dermis for morphology check to determine the hair cycle stages.

Temporal cell cycle pulsing

To determine HFSC proliferation rate, EdU incorporation was performed to label stem cells that were undergoing proliferation. Male and female *CD1* mice were injected with 5'-ethynyl-2'-deoxyuridine (EdU) (Sigma & Medchemexpress LLC) intraperitoneally (312.5 μg per injection) 24 hours, 12 hours, and 10 min before (total of 3 doses) the analysis.

Label retaining assay

To trace HFSC proliferation history, EdU incorporation was performed to track the label-retaining stem cells after a full hair cycle. Male and female *CD1* mice were injected intraperitoneally (312.5 μg per injection) twice a day from 1st telogen to early Ana III or late Ana III with 5'-ethynyl-2'-deoxyuridine (EdU) (Sigma & Medchemexpress LLC). Mice were traced and analyzed at 2nd telogen.

Hair follicle stem cell clone lineage tracing

Mice used for HFSC clone lineage tracing experiments were *Sox9-CreER^{+};Brainbow^{fl}*, *Sox9-CreER^{+};YFP^{fl}*, inducible CreER driven *Sox9* promoter with the administration of Tamoxifen (TAM) intraperitoneally. *Sox9-CreER$^{+/-}$;Brainbow$^{fl/-}$* and *Sox9-CreER$^{+/-}$;YFP$^{fl/-}$* mice were given 1 dose of TAM (Sigma) in corn oil (Fisher Scientific) (0.03 mg for *Sox9-CreER$^{+/-}$;Brainbow$^{fl/-}$* or 0.01 mg for *Sox9-CreER$^{+/-}$;YFP$^{fl/-}$*) at 1st telogen (P19 or P20). Mice were monitored and sacrificed between Ana III to 2nd telogen.

Lymphatic vessels ablation

Mice used for lymphatics ablation experiments were *Prox1-CreER^{+};iDTR$^{fl/fl}$*, TAM-inducible CreER driven *Prox1* gene of lymphatic endothelium, expressing diphtheria toxin receptor (DTR), allowing lymphatic endothelium ablation followed by diphtheria toxin (DT) administration. TAM injections were given 1 dose (50 μl of 20 mg/ml) every other two days starting at P20 for a total of 3 doses. For lymphatic vessel depletion, mice were injected with 3 doses (40 ng/mouse) intradermally of DT (Sigma) under anesthesia for 2 consecutive days following TAM injections. Mice were monitored post-DT administration and littermates were assigned to experimental (with DT injections) and control groups (with 1X PBS injections with replacement of DT injection procedure). For acute lymphatic collapse experiments, *Sox9-CreER$^{+/-}$*

;Brainbow$^{fl/-}$ mice were injected intradermally with either VEGFR3-Fc chimera (10 µg in 10 µl volume; R&D) or 1X PBS for consecutive 3 days for P24 to P26 under anesthesia after the TAM administration at P20.

Op-Puro translation assay

CD1 mice were injected with OP-puromycin (Op-Puro; 50 mg/kg; gifted by Signer Lab) intraperitoneally 1 hour before euthanasia at P19 (1st telogen) and P21 (Ana III).

Esophageal epithelium-skin stroma tissue co-culture

<u>*Skin Dermis*</u>: Back skin dermis was obtained from the *Prox1-CreER*$^{+}$*;iDTR*$^{fl/fl}$ mice at 2nd telogen with lymphatics ablation procedure listed in the previous session as an experimental group, or the *Prox1-CreER*$^{+}$*;iDTR*$^{fl/fl}$ mice without DT injection as the control group. To remove the HF and skin epidermis, the fixed obtained back skin was incubated (dermis side down) on 2.5 U/ml dispase II (Fisher Scientific) + 19.23 mM EDTA (Fisher Scientific) for at least 2 hours at 37°C on a shaker and peeled completely with only skin dermis retained.

<u>*Esophageal epithelium*</u>: Esophageal epithelium was obtained from the *UBC-GFP* mice. The esophagus was flattened by dissecting from the tube center and placed in 5 mM EDTA at 37°C for 3-4 hours to remove the esophageal stroma (Bejar et al., 2021).

<u>*Co-culture*</u>: Referring to Bejar et al., 2021, the esophageal epithelium was embedded directly onto the skin dermis, and then they were placed onto 6.5 mm Transwell® with 8.0 µm Pore Polycarbonate Membrane Insert (Corning) in 24 well-plate, and incubated at 37°C for 5 min for attachment. Then the co-culture tissues were covered by the 500 µl media containing DMEM (4.5 g/L D-Glucose, L-Glutamine), 110 mg/L (1 mM) Pyruvate, DMEM/F12 (55 mg/L (0.5 mM) Pyruvate), 5 µg/ml 3,3',5-Triiodothyroacetic acid, 0.18 mM Adenine, 8 µg/ml transferrin, and 5%

Penicillin-Streptomycin. The co-culture tissues were grown for 10 days at 37°C and 7.5% CO2, and the media was replaced on alternate days.

Immunofluorescence

Hair follicle whole mount: Mouse back skin was collected and its subcutaneous fat was removed; then the skin was incubated on 2 U/ml dispase II + 19.23 mM EDTA with the same procedure used for hair cycle timing to obtain HFs from the skin dermis. The peeled HFs were fixed in 4% PFA for 10 min at room temperature (RT). The HFs were then washed 3 times with 1X PBS before being permeabilized in PBS + 0.3% Triton (PBST) for 1 hour at RT. Primary antibodies in PBST were added to the samples and incubated overnight at RT on a shaker. The following primary antibodies were used: anti-P-CAD (1:500, R&D AF761), anti-Sox9 (1:500, Sigma AB5535), anti-KRT24 (1:3000, gifted by Fuchs Lab). Samples were then washed 3 times with 1X PBS for 10 min each at RT the following day. Secondary antibodies in PBST were next added to the samples and incubated for 2 hours at RT on a shaker. The following secondary antibodies were used: Donkey anti-goat RRX (1:1000, Jackson Immunoresearch 705-295-147), Donkey anti-rabbit Alexa 488 (1:1000, Jackson Immunoresearch 711-545-152), Donkey anti-rabbit Alexa 647 (1:1000, Jackson Immunoresearch 711-605-152), DAPI (1:1000 Sigma D9542). Samples were then washed with PBST + 1:1000 DAPI 3 times for 10 min each at RT. EdU Click-iT reaction was next performed according to the manufacturer's instructions (Invitrogen™ Thermo Fisher), then washed with PBST 3 times for 10 min each at RT. HFs were separated from the epidermis on Superfrost™ Plus Microscope Slides (Fisher Scientific) and mounted with ProLong Gold Antifade Mountant (Thermo Fisher Scientific).

Skin sections: Mouse back skin was dissected with its subcutaneous fat removed, and placed on Whatman paper in 4% PFA for 1 hour at RT with epidermis side down for fixation. Skin

samples were then washed 3 times with 1X PBS for 30 min each. Next, the samples were incubated in 30% sucrose for 48 hour on a shaker at 4°C followed by embedding in OCT (Fisher Scientific) and stored at -80°C. Frozen tissue blocks were sectioned at 25 µm on a cryostat (Leica), and mounted on Superfrost™ Plus Microscope Slides (Fisher Scientific). The sections were then blocked for 1 hour at RT in blocking buffer (1% bovine serum albumin (Sigma, A2153- 100G), 1% fish gelatin (Sigma, G7765- 1L), 2.5% normal donkey serum (Jackson Immunoresearch, 017-000-121), 0.3% TritonX-100 (Sigma, T8787- 250ML) in 1X PBS). Sections were then incubated in primary antibodies diluted in blocking buffer overnight at 4°C. The following primary antibodies were used: anti-P-CAD (1:800, R&D AF761), anti-LYVE (1:600, AngioBio 11-034), anti-KRT24 (1:3000, gifted by Fuchs Lab), anti-LYVE (1:600, Thermo Fisher 14-0443-82), anti-GFP (1:2000, Fisher 501058132), Anti-RFP (1:1000, MyBioSource MBS448122), anti-K5 (1:800, Biolegend 905903). Sections were next washed 3 with 1X PBS, followed by secondary antibodies incubation for 2 hours at RT. The following secondary antibodies were used: Donkey anti-goat RRX (1:1000, Jackson Immunoresearch 705-295-147), Donkey anti-rat RRX (1:1000, Jackson Immunoresearch 712-295-153), Donkey anti-rabbit RRX (1:1000, Jackson Immunoresearch 295-152), Donkey anti-rabbit Alexa 488 (1:1000, Jackson Immunoresearch 711-545-152), Donkey anti-chicken Alexa 488 (1:1000, Jackson Immunoresearch 703-545-155), Donkey anti-rat Alexa 488 (1:1000, Jackson Immunoresearch 545-150), Donkey anti-rabbit Alexa 647 (1:1000, Jackson Immunoresearch 711-605-152), Donkey anti-rabbit Alexa 405 (1:1300, Abcam ab175651), DAPI (1:1000 Sigma D9542). EdU and Op-Puro Click-iT reactions were next performed according to the manufacturer's instructions (Invitrogen™ Thermo Fisher), then washed with PBST 3 times for 10 min each at RT, and mounted with ProLong Gold Antifade Mountant (Thermo Fisher Scientific).

Skin whole mount: Mouse back skin was dissected with its subcutaneous fat removed, and placed on Whatman paper in 4% PFA for 1 hour at RT with epidermis side down for fixation. Skin samples were then washed 3 times with 1X PBS for 30 min each. Next, the Whatman paper was removed from the samples and the samples were incubated in 0.3% PBST overnight at RT on a shaker, followed by adding primary antibodies diluted in 0.3% PBST the next day and incubating them overnight at RT on a shaker. The following primary antibodies were used: anti-KRT24 (1:2000, gifted by Fuchs Lab), anti-LYVE (1:300, Thermo Fisher 14-0443-82), anti-GFP (1:1000, Fisher 501058132), Anti-RFP (1:500, MyBioSource MBS448122), anti-VEGFR3 (1:300, Biotechne AF743- SP). The samples were washed with 0.3% PBST 3 times for 30 min each. Then the samples were incubated in secondary antibodies overnight at RT on a shaker. The following secondary antibodies were used: Donkey anti-goat RRX (1:500, Jackson Immunoresearch 705-295-147), Donkey anti-rat RRX (1:500, Jackson Immunoresearch 712-295-153), Donkey anti-chicken Alexa 488 (1:500, Jackson Immunoresearch 703-545-155), Donkey anti-rabbit Alexa 647 (1:500, Jackson Immunoresearch 711-605-152), Donkey anti-goat Alexa 405 (1:500, Thermo Scientific A48259), DAPI (1:700 Sigma D9542). The samples were washed with 0.3% PBST + 1:1000 DAPI 3 times for 30 each at RT on a shaker and proceeded to tissue clearing.

Tissue clearing: The whole mount-stained back skin tissues were placed in increasing concentrations of ethanol DI water: 30%, 50%, 70%, and 100% in order with adjected pH 9.0 for 1 hour each at RT on shaker for dehydration. The 100% ethanol was switched to another round of 100% ethanol overnight at RT on a shaker. Next, each sample was transferred into an individual Eppendorf tube with 1 ml ethyl cinnamate (Sigma) and shaken on a shaker overnight at RT for clearing (Gur-Cohen et al., 2019; Klingberg et al., 2017).

Confocal microscopy and image processing

All samples were imaged under the Andor Dragonfly Spinning Disk Confocal. EdU^+ label-retaining cell quantification and clone fate identification were processed using the Imaris software. Intensity quantification for Op-Puro was processed using Fiji.

Statistical significance was measured using paired T-tests for experiments with 2 groups. One-way ANOVA and two-way ANOVA with Tukey Comparisons were performed for experiments with more than 2 groups for comparison. Alpha values under $p < 0.05$ were determined statistically significant.

REFERENCES

Alonso, L., & Fuchs, E. (2006). The hair cycle. *Journal of Cell Science*, *119*(3), 391–393. https://doi.org/10.1242/jcs.02793

Aponte, P. M., & Caicedo, A. (2017). Stemness in Cancer: Stem Cells, Cancer Stem Cells, and Their Microenvironment. *Stem Cells International*, *2017*, 1–17. https://doi.org/10.1155/2017/5619472

Batlle, E., & Clevers, H. (2017). Cancer stem cells revisited. *Nature Medicine*, *23*(10), 1124–1134. https://doi.org/10.1038/nm.4409

Bejar, M. T., Jimenez-Gomez, P., Moutsopoulos, I., Colom, B., Han, S., Calero-Nieto, F. J., Göttgens, B., Mohorianu, I., Simons, B. D., & Alcolea, M. P. (2021). *Defining the transcriptional signature of esophageal-to-skin lineage conversion*. https://doi.org/10.1101/2021.02.19.431899

Blanpain, C., & Fuchs, E. (2014). Plasticity of epithelial stem cells in tissue regeneration. *Science*, *344*(6189), 1242281. https://doi.org/10.1126/science.1242281

Buck, S. B., Bradford, J., Gee, K. R., Agnew, B. J., Clarke, S. T., & Salic, A. (2008). Detection of S-phase cell cycle progression using 5-ethynyl-2′-deoxyuridine incorporation with click chemistry, an alternative to using 5-bromo-2′-deoxyuridine antibodies. *BioTechniques*, *44*(7), 927–929. https://doi.org/10.2144/000112812

Chen, L., Zhang, M., Li, H., Tang, S., & Fu, X. (2014). Distribution of BrdU label-retaining cells in eccrine sweat glands and comparison of the percentage of BrdU-positive cells in eccrine sweat glands and in epidermis in rats. *Archives of Dermatological Research*, *306*(2), 157–162. https://doi.org/10.1007/s00403-013-1397-7

Cotsarelis, G., Sun, T.-T., & Lavker, R. M. (1990). Label-retaining cells reside in the bulge area of pilosebaceous unit: Implications for follicular stem cells, hair cycle, and skin carcinogenesis. *Cell*, *61*(7), 1329–1337. https://doi.org/10.1016/0092-8674(90)90696-C

Ferraro, F., Celso, C. L., & Scadden, D. (2010). Adult Stem Cels and Their Niches. In E. Meshorer & K. Plath (Eds.), *The Cell Biology of Stem Cells* (Vol. 695, pp. 155–168). Springer US. https://doi.org/10.1007/978-1-4419-7037-4_11

Fuchs, E., & Blau, H. M. (2020). Tissue Stem Cells: Architects of Their Niches. *Cell Stem Cell*, *27*(4), 532–556. https://doi.org/10.1016/j.stem.2020.09.011

Fuller, M. T., & Spradling, A. C. (2007). Male and Female *Drosophila* Germline Stem Cells: Two Versions of Immortality. *Science*, *316*(5823), 402–404. https://doi.org/10.1126/science.1140861

Goodell, M. A., & Rando, T. A. (2015). Stem cells and healthy aging. *Science*, *350*(6265), 1199–1204. https://doi.org/10.1126/science.aab3388

Goto, N., Goto, S., Imada, S., Hosseini, S., Deshpande, V., & Yilmaz, Ö. H. (2022). Lymphatics and fibroblasts support intestinal stem cells in homeostasis and injury. *Cell Stem Cell*, *29*(8), 1246-1261.e6. https://doi.org/10.1016/j.stem.2022.06.013

Gur-Cohen, S., Yang, H., Baksh, S. C., Miao, Y., Levorse, J., Kataru, R. P., Liu, X., De La Cruz-Racelis, J., Mehrara, B. J., & Fuchs, E. (2019). Stem cell–driven lymphatic remodeling coordinates tissue regeneration. *Science*, *366*(6470), 1218–1225. https://doi.org/10.1126/science.aay4509

Hsu, Y.-C., Pasolli, H. A., & Fuchs, E. (2011). Dynamics between Stem Cells, Niche, and Progeny in the Hair Follicle. *Cell*, *144*(1), 92–105. https://doi.org/10.1016/j.cell.2010.11.049

Ito, M., Liu, Y., Yang, Z., Nguyen, J., Liang, F., Morris, R. J., & Cotsarelis, G. (2005). Stem cells in the hair follicle bulge contribute to wound repair but not to homeostasis of the epidermis. *Nature Medicine*, *11*(12), 1351–1354. https://doi.org/10.1038/nm1328

Jahoda, C. A. B., Horne, K. A., & Oliver, R. F. (1984). Induction of hair growth by implantation of cultured dermal papilla cells. *Nature*, *311*(5986), 560–562. https://doi.org/10.1038/311560a0

Junyent, S., Meglicki, M., Vetter, R., Mandelbaum, R., King, C., Patel, E. M., Iwamoto-Stohl, L., Reynell, C., Chen, D.-Y., Rubino, P., Arrach, N., Paulson, R. J., Iber, D., & Zernicka-Goetz, M. (2024). The first two blastomeres contribute unequally to the human embryo. *Cell*, *187*(11), 2838-2854.e17. https://doi.org/10.1016/j.cell.2024.04.029

Kiel, M. J., Yilmaz, Ö. H., Iwashita, T., Yilmaz, O. H., Terhorst, C., & Morrison, S. J. (2005). SLAM Family Receptors Distinguish Hematopoietic Stem and Progenitor Cells and Reveal Endothelial Niches for Stem Cells. *Cell*, *121*(7), 1109–1121. https://doi.org/10.1016/j.cell.2005.05.026

Klingberg, A., Hasenberg, A., Ludwig-Portugall, I., Medyukhina, A., Männ, L., Brenzel, A., Engel, D. R., Figge, M. T., Kurts, C., & Gunzer, M. (2017). Fully Automated Evaluation of Total Glomerular Number and Capillary Tuft Size in Nephritic Kidneys Using Lightsheet Microscopy. *Journal of the American Society of Nephrology*, *28*(2), 452–459. https://doi.org/10.1681/ASN.2016020232

Kusumbe, A. P., Ramasamy, S. K., Itkin, T., Mäe, M. A., Langen, U. H., Betsholtz, C., Lapidot, T., & Adams, R. H. (2016). Age-dependent modulation of vascular niches for haematopoietic stem cells. *Nature*, *532*(7599), 380–384. https://doi.org/10.1038/nature17638

Laplane, L., & Solary, E. (2019). Towards a classification of stem cells. *eLife*, *8*, e46563. https://doi.org/10.7554/eLife.46563

Li, K. N., & Tumbar, T. (2021). Hair follicle stem cells as a skin-organizing signaling center during adult homeostasis. *The EMBO Journal*, *40*(11), e107135. https://doi.org/10.15252/embj.2020107135

Liu, J., Xu, Y., Stoleru, D., & Salic, A. (2012). Imaging protein synthesis in cells and tissues with an alkyne analog of puromycin. *Proceedings of the National Academy of Sciences*, *109*(2), 413–418. https://doi.org/10.1073/pnas.1111561108

Mäkinen, T., Jussila, L., Veikkola, T., Karpanen, T., Kettunen, M. I., Pulkkanen, K. J., Kauppinen, R., Jackson, D. G., Kubo, H., Nishikawa, S.-I., Ylä-Herttuala, S., & Alitalo, K. (2001). Inhibition of lymphangiogenesis with resulting lymphedema in transgenic mice expressing soluble VEGF receptor-3. *Nature Medicine*, *7*(2), 199–205. https://doi.org/10.1038/84651

Marusyk, A., & DeGregori, J. (2008). Declining cellular fitness with age promotes cancer initiation by selecting for adaptive oncogenic mutations. *Biochimica et Biophysica Acta (BBA) - Reviews on Cancer*, *1785*(1), 1–11. https://doi.org/10.1016/j.bbcan.2007.09.001

Mimeault, M., & Batra, S. K. (2008). Recent Progress on Tissue-Resident Adult Stem Cell Biology and Their Therapeutic Implications. *Stem Cell Reviews*, *4*(1), 27–49. https://doi.org/10.1007/s12015-008-9008-2

Morris, R. J., Liu, Y., Marles, L., Yang, Z., Trempus, C., Li, S., Lin, J. S., Sawicki, J. A., & Cotsarelis, G. (2004). Capturing and profiling adult hair follicle stem cells. *Nature Biotechnology*, *22*(4), 411–417. https://doi.org/10.1038/nbt950

Morrison, S. J., & Spradling, A. C. (2008). Stem Cells and Niches: Mechanisms That Promote Stem Cell Maintenance throughout Life. *Cell*, *132*(4), 598–611. https://doi.org/10.1016/j.cell.2008.01.038

Niec, R. E., Chu, T., Schernthanner, M., Gur-Cohen, S., Hidalgo, L., Pasolli, H. A., Luckett, K. A., Wang, Z., Bhalla, S. R., Cambuli, F., Kataru, R. P., Ganesh, K., Mehrara, B. J., Pe'er, D., & Fuchs, E. (2022). Lymphatics act as a signaling hub to regulate intestinal stem cell activity. *Cell Stem Cell*, *29*(7), 1067-1082.e18. https://doi.org/10.1016/j.stem.2022.05.007

Oliver, G. (2004). Lymphatic vasculature development. *Nature Reviews Immunology*, *4*(1), 35–45. https://doi.org/10.1038/nri1258

Oliver, G., Kipnis, J., Randolph, G. J., & Harvey, N. L. (2020). The Lymphatic Vasculature in the 21st Century: Novel Functional Roles in Homeostasis and Disease. *Cell*, *182*(2), 270–296. https://doi.org/10.1016/j.cell.2020.06.039

Palikuqi, B., Rispal, J., Reyes, E. A., Vaka, D., Boffelli, D., & Klein, O. (2022). Lymphangiocrine signals are required for proper intestinal repair after cytotoxic injury. *Cell Stem Cell*, *29*(8), 1262-1272.e5. https://doi.org/10.1016/j.stem.2022.07.007

Peña-Jimenez, D., Fontenete, S., Megias, D., Fustero-Torre, C., Graña-Castro, O., Castellana, D., Loewe, R., & Perez-Moreno, M. (2019). Lymphatic vessels interact dynamically with the hair follicle stem cell niche during skin regeneration *in vivo*. *The EMBO Journal*, *38*(19), e101688. https://doi.org/10.15252/embj.2019101688

Prager, B. C., Xie, Q., Bao, S., & Rich, J. N. (2019). Cancer Stem Cells: The Architects of the Tumor Ecosystem. *Cell Stem Cell*, *24*(1), 41–53. https://doi.org/10.1016/j.stem.2018.12.009

Putnam, A. J. (2014). The instructive role of the vasculature in stem cell niches. *Biomater. Sci.*, *2*(11), 1562–1573. https://doi.org/10.1039/C4BM00200H

Rompolas, P., Deschene, E. R., Zito, G., Gonzalez, D. G., Saotome, I., Haberman, A. M., & Greco, V. (2012). Live imaging of stem cell and progeny behaviour in physiological hair-follicle regeneration. *Nature*, *487*(7408), 496–499. https://doi.org/10.1038/nature11218

Rompolas, P., Mesa, K. R., & Greco, V. (2013). Spatial organization within a niche as a determinant of stem-cell fate. *Nature*, *502*(7472), 513–518. https://doi.org/10.1038/nature12602

Tammela, T., & Alitalo, K. (2010). Lymphangiogenesis: Molecular Mechanisms and Future Promise. *Cell*, *140*(4), 460–476. https://doi.org/10.1016/j.cell.2010.01.045

Tian, Z., Yu, T., Liu, J., Wang, T., & Higuchi, A. (2023). Introduction to stem cells. In *Progress in Molecular Biology and Translational Science* (Vol. 199, pp. 3–32). Elsevier. https://doi.org/10.1016/bs.pmbts.2023.02.012

Yamashita, Y. M., Yuan, H., Cheng, J., & Hunt, A. J. (2010). Polarity in Stem Cell Division: Asymmetric Stem Cell Division in Tissue Homeostasis. *Cold Spring Harbor Perspectives in Biology*, *2*(1), a001313–a001313. https://doi.org/10.1101/cshperspect.a001313

Yang, H., Adam, R. C., Ge, Y., Hua, Z. L., & Fuchs, E. (2017). Epithelial-Mesenchymal Micro-niches Govern Stem Cell Lineage Choices. *Cell*, *169*(3), 483-496.e13. https://doi.org/10.1016/j.cell.2017.03.038

Zhang, L., Li, H., Zeng, S., Chen, L., Fang, Z., & Huang, Q. (2015). Long-term tracing of the BrdU label-retaining cells in adult rat brain. *Neuroscience Letters*, *591*, 30–34. https://doi.org/10.1016/j.neulet.2015.02.023